ARTICLE

Novel thermally activated delayed fluorescence materials by high-throughput virtual screening: going beyond donor-acceptor design†

Received 00th January 20xx,
Accepted 00th January 20xx

DOI: 10.1039/x0xx00000x

Ke Zhao, *[a] Ömer H. Omar, [b] Tahereh Nematiaram, [b] Daniele Padula [c] and Alessandro Troisi *[b]

A series of candidates of thermally activated delayed fluorescence (TADF) materials, which have important applications in organic light emitting diodes devices, are identified by a high-throughput virtual screening of a database of known molecular materials. The first step of the screening identifies nearly 700 molecules that, in the X-ray geometry, have a sufficiently small gap between excitation energy of the lowest singlet and triplet states and acceptable oscillator strength of the singlet. After geometry optimization, 125 molecules continue to satisfy the energy criteria for potential TADF. Furthermore, the parameters of excited state dynamics including the reorganization energy, adiabatic excitation energy and spin-orbital coupling are calculated for a sample of molecules based on the optimized excited state geometries. The majority of the candidates are not known as TADF materials and could be considered promising lead compounds for the exploration of this materials class. Interestingly, it is found that some novel chromophores deviate from the current design rule for TADF materials, which are invariably based on a donor-acceptor molecular architecture. We also illustrate how to design completely new types of TADF materials using the results of this screening.

Introduction

Thermally activated delayed fluorescence (TADF) is an interesting radiative transition phenomenon which occurs in photoluminescence or electroluminescence processes.[1-3] In electroluminescence, the non-emissive triplet state exciton could transmit to the emissive singlet state by reverse intersystem crossing (RISC) under thermal activation, and then emit via delayed fluorescence. Due to harvesting both singlet and triplet excitons, 100% internal quantum efficiency can be achieved in TADF emitters. Since Adachi et al. reported TADF-based highly efficient organic light emitting diodes (OLED) devices in 2012,[4] great research efforts have been devoted to the design and application of the TADF materials.[5-8]

It has been known that the energy gap (ΔE_{ST}) between the lowest singlet excited state (S_1) and triplet excited state (T_1) is the key parameter for the design of TADF emitters.[3,5,6] A very small ΔE_{ST} can enhance $T_1 \rightarrow S_1$ RISC efficiency. In addition, the oscillator strength of the S_1 to the ground state S_0 (f) needs to be maximized in order to facilitate the draining of S_1.[3,5] The small ΔE_{ST} is usually achieved by designing molecules with a twisted electron donor-acceptor structure (e.g. with the dihedral angle between the donor and acceptor planes in the range of 70°-90°).[9] In this case, the overlap of the molecule's orbitals, the highest occupied molecular orbital (HOMO) and the lowest unoccupied molecular orbital (LUMO) decreases and the exchange energy, which determines ΔE_{ST}, is expected to be reduced correspondingly. However, the reduced HOMO-LUMO overlap would also result in the decrease of transition dipole momentum, which would lead to smaller oscillator strengths.[10,11] Therefore, the donor, acceptor and linker of a TADF emitter need to be carefully modulated to achieve the balance of both requirements. The donor and the acceptor are conventionally connected by a twisted, bulky or spiro junction which can provide a large steric hindrance for effective separation of HOMO and LUMO.[2]

Although many studies have revealed that donor-acceptor design is a successful approach to develop TADF emitters, researchers have been exploring alternative strategies.[7,11-13] Recently, Chen and co-workers reported a new design strategy for combining a small ΔE_{ST} with a large oscillator strength, which opens a way for coplanar molecules to be efficient TADF emitters.[11] Hatakeyama et al. proposed a new structure that contains a rigid boron-nitrogen framework.[12] Making use of the opposite resonance effect of the boron and nitrogen atoms, the separation of HOMO and LUMO is achieved without introducing donor or acceptor groups. The local excitonic triplet state and the contributions of multiple electronic configurations were involved in the construction of these new design strategies.[11,13] The aim of this work is to screen a high number of known molecules for potential TADF activity, without any structural constraint imposed a priori, to identify new TADF molecules that will suggest new design rules.

There are many successful recent examples of the high-throughput virtual screening (HTVS) method[14] applied to the design of optoelectronic materials.[15-17] Shu et al. presented a flexible approach to automated material design and applied it to

[a] School of Physics and Electronics, Shandong Normal University, Jinan, 250358, China. E-mail: zhaoke@sdnu.edu.cn
[b] Department of Chemistry and Materials Innovation Factory, University of Liverpool, Liverpool, L69 7ZD, U.K. E-mail: a.troisi@liverpool.ac.uk
[c] Dipartimento di Biotecnologie, Chimica e Farmacia, Università di Siena, via A. Moro 2, Siena, 53100, Italy.
†Electronic Supplementary Information (ESI) available: Calibration, convergence problem, molecular design, and information of candidates. See DOI: 10.1039/x0xx00000x

This is a peer-reviewed, accepted author manuscript of the following article: Nematiaram, T. (2021). Novel thermally activated delayed fluorescence materials by high-throughput virtual screening: going beyond donor–acceptor design. Journal of Materials Chemistry C, 2021(9), 3324-3333. https://doi.org/10.1039/d1tc00002k

search through a large chemical space for TADF molecules.[15] Each molecule in their defined space has a central electron acceptor group surrounded by a combination of electron donating and electron withdrawing groups. Gómez-Bombarelli and co-workers also performed a HTVS combined with an experimental approach for the design of efficient TADF molecules.[16] Their molecular search space was a virtual chemical library which followed the donor-(bridge)$_n$-acceptor architecture where n was 0, 1 or 2. Therefore, both examples considered the search space consisting of artificial systems with donor and acceptor moieties and their searches for new TADF candidates had to follow the known design rule, since it was imposed a priori. A possible approach to search for more diverse structures and discover new design rules can be based on screening a database of known molecular materials such as the Cambridge Structural Database (CSD).[18] This approach was followed to search for potential singlet fission molecules and to discover design principles for reducing the dynamic disorder in molecular semiconductors.[19] After computing the excited state energy for 40000 organic semiconducting molecules in their X-ray geometries, several hundreds of candidates were chosen for optimization and accurate calculations (such database was derived from approximately one million structures in the CSD). Many of the discovered potential singlet fission molecules were not previously known for this property, illustrating the power of virtual screening protocols that do not restrict the chemical space. In the remainder of this paper, we present the screening protocol that we have devised for the discovery of new potential TADF candidates, a detailed analysis of the results with emphasis on the more novel aspects of the findings and a few examples on how the results of this work could be used to design new molecules. Furthermore, for a subset of potential candidates, we evaluate the parameters affecting the excited state dynamics of interest.

Virtual screening

An outline of the overall virtual screening process is illustrated in Fig. 1. The vertical excitation energies of S_1 and T_1 on the crystallographic X-ray geometry were computed in our previous work.[19] Nearly seven hundred molecules have a sufficiently small energy gap between S_1 and T_1 and acceptable oscillator strength of S_1, and then their geometries of ground state are optimized and the vertical excitation energies of S_1 and T_1 are calculated on optimized S_0 state. After geometry optimization, 125 molecules continue to satisfy the energy criteria for potential TADF and their spin-orbital couplings (SOC) are computed. Among these 125 candidates, 28 molecules are selected as samples for the excited state optimization. The reorganization energy, adiabatic excitation energy, and SOC are calculated on optimized S_1 and T_1 geometries.

The vertical excitation energies of S_1 and T_1 on the X-ray geometry are denoted as $E_x(S_1)$ and $E_{x,scf}(T_1)$ or $E_{x,td}(T_1)$ computed via a ΔSCF procedure or TDDFT, respectively. Geometry optimization for the ground state is performed for a selected number of molecules and the corresponding excitation energies are indicated as $E_o(S_1)$, $E_{o,scf}(T_1)$ or $E_{o,td}(T_1)$. The BLYP35 functional with the large, def2-TZVP basis set is used for optimization and the TDDFT calculations at M06-2X/def2-

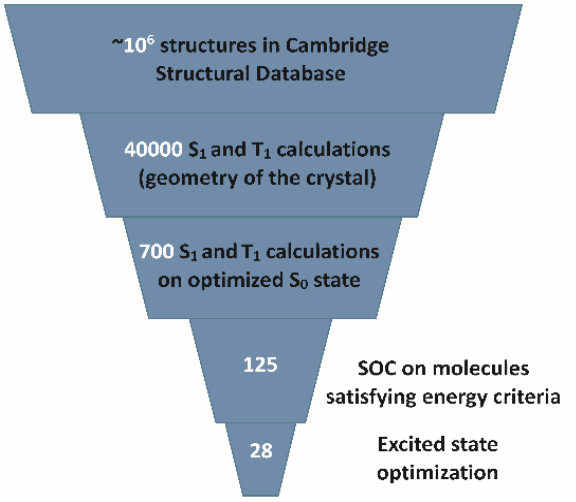

Fig. 1 The computational funnel for overall virtual screening considered in this work.

TZVP level of theory as implemented in Gaussian 16[20] are employed to evaluate $E_o(S_1)$ and $E_{o,td}(T_1)$.[21] A ΔSCF procedure at the same level of the theory is used to obtain $E_{o,scf}(T_1)$. The computational methods were proposed in ref. 21 and have been verified its quality in our previous work.[19] Comparison between a set of computed and experimental excitation energies was used to extract a linear calibration between the two (Fig. S1, ESI†). The calibrated energies are indicated with a prime superscript and the calibration used was (energy expressed in eV):

$$E_o(S_1)'=0.7502E_o(S_1)+0.3269 \quad (1)$$

$$E_{o,scf}(T_1)'=0.7130E_{o,scf}(T_1)+0.0534 \quad (2)$$

$$E_{o,td}(T_1)'=0.7901E_{o,td}(T_1)+0.0626 \quad (3)$$

The excitation energies calibrated as above but computed from the X-ray geometry are indicated as $E_x(S_1)'$, $E_{x,scf}(T_1)'$ and $E_{x,td}(T_1)'$.

Our strategy is to use the available $E_x(S_1)'$, $E_{x,scf}(T_1)'$ and $E_{x,td}(T_1)'$ to extract a long-list of plausible candidates for TADF on the basis of a sufficiently small energy difference between T_1 and S_1 states and excluding molecules with too low oscillator strength of S_1. The initial criteria are chosen to be relatively lenient and have been adjusted to yield a sufficiently small set of preliminary candidates which can be evaluated at the desired level of accuracy. To identify the initial long-list, we used two different strategies: 1) We extracted a list of 526 molecules which satisfy the criteria $E_x(S_1)'-E_{x,scf}(T_1)'<0.48$ eV and $f>0.02$; 2) We extracted a list of 324 molecules that satisfy the criteria $E_x(S_1)'-E_{x,td}(T_1)'<0.48$ eV and $f>0.02$. The two approaches are necessary because, while ΔSCF triplets are slightly more accurate, they may occasionally converge on an excited state, giving a large number of false positives that emerged during the manual examination of some elements in the long-list (Fig. S2, ESI†). We also noticed a few instances where molecules formed by weakly interacting identical conjugated fragments had multi-configurational triplets that could not be studied accurately within an unrestricted SCF calculation (Fig. S2, ESI†).

We obtain a set of 698 molecules that satisfied one of the criteria above and could be optimized without error. After geometry optimization, as the reduced database is still too large

for manually inspecting all results, we analysed the potential TADF molecules on the basis of the more robust TDDFT (calibrated) calculations, i.e. $E_o(S_1)'$ and $E_{o,td}(T_1)'$. Fig. 2 presents the overall molecular distribution in the range of $0<\Delta E_{ST}=E_o(S_1)'-E_{o,td}(T_1)'<0.8$ eV. Using a stacked-bar representation, the number of molecules in each energy gap interval is classified into two groups: the one with $f>0.02$ highlighted in blue and the one with $f<0.02$ highlighted in orange. When the energy gap ΔE_{ST} is small, the percentage of the molecules with $f<0.02$ is large. In the range of 0.15-0.2 eV, only 1 out 8 molecules has $f>0.02$. This demonstrates that the decrease in energy gap results in smaller oscillator strengths, as expected.[10,11]

To set reasonable criteria for selecting the potential TADF molecules from the 698 molecules, we calculated excited state energies of 10 experimentally known TADF molecules using the same method and calibration and compared with experimental data (Table 1). All the calculated energy gaps ΔE_{ST} are less than 0.4 eV except for DMOC-DPS. The experimental values are very small and less than 0.25 eV, which is the range of the majority of experimentally observed TADF molecules.[5] This indicates that our computational method and calibration tends to overestimate the energy gap of TADF active molecules. In fact, the calibration performed with ~100 experimental evaluation of singlet and triplet excitation energies suggest a root mean squared error (RMSE) of ~50 meV on each (Fig. S1, ESI†). The RMSE on their difference in Table 1 is 130 meV, i.e. slightly larger than expected and skewed toward larger gaps because of correlation between error in S_1 and T_1 energies. However, such systematic error can be corrected and, from the data in Table 1, TADF candidates can be chosen to have ΔE_{ST} <0.4 eV for the particular choice of computational methods. It should be mentioned that the database of 40000 molecules was derived without any consideration for TADF and no criterion was imposed on it. So, the best possible experimental validation of the prediction consists in the method being able to "rediscover" the TADF active molecules. When the criterion is set to be ΔE_{ST} <0.4 eV, 125 potential TADF candidates (Table S1 and S2, ESI†) can be identified from the 698 molecules. In particular, 0.3% of the initial database of 40000 molecules was predicted to be TADF active and one third of this (~0.1% of the total) are either known TADF or closely related molecules (as discussed in the next session). These data confirm the effectiveness of the screening.

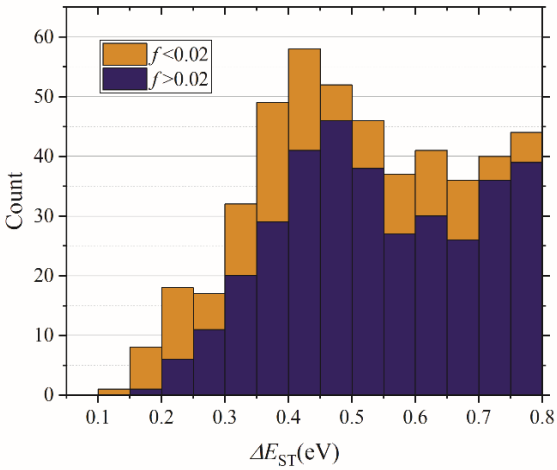

Fig. 2 The number of molecules in different range of energy gap. The blue and orange bars denote the number of the molecules with $f>0.02$ and $f<0.02$, respectively.

As for the oscillator strength, since most of these TADF molecules have very small oscillator strengths (near to zero), no additional oscillator strength criterion is imposed in this stage. In addition, we plotted the relation between calibrated excitation energy of S_1 and T_1 for X-ray and optimized structures for the total 698 molecules and the 125 candidates (Fig. S3 and S4, ESI†). There is generally a good agreement between X-ray and optimized structures suggesting that the approach of pre-screening using X-ray geometry is a valid one. At the same time, the fraction of molecules that miss the criterion after optimization is too large and one cannot rely on the X-ray geometry for a fully predictive approach.

Molecules with small singlet-triplet gap

We focus initially on the analysis of molecules with small singlet-triplet gap ΔE_{ST}, which is one of the most challenging properties for efficient energy conversion between S_1 and T_1.[5] The 125 potential TADF candidates are grouped into seven different types with increasing level of deviation from the common chemistry of known TADF materials. These molecules are discussed in the rest of this section in terms of their chemical and electronic structure. The calibrated excitation energy $E_o(S_1)'$

Table 1 The calculated excited state energies $E_o(S_1)$ and $E_{o,td}(T_1)$, the calibrated energies $E_o(S_1)'$ and $E_{o,td}(T_1)'$, the energy gap $\Delta E_{ST}=E_o(S_1)'-E_{o,td}(T_1)'$ and the oscillator strength f for 10 TADF molecules. The data in parentheses are the experimental values from refs. 4 and 22-30. The labels of the compounds in the first column are those used in the references given.

TADF molecules	$E_o(S_1)$(eV)	$E_{o,td}(T_1)$(eV)	$E_o(S_1)'$(eV)	$E_{o,td}(T_1)'$(eV)	ΔE_{ST} (eV)	f
DMOC-DPS	3.8066	3.2193	3.1826	2.6062	0.5764 (0.21)[22]	0.599
DMAC-DPS	3.6171	3.6105	3.0404	2.9153	0.1251 (0.08)[23]	0
DMAC-TRZ	3.4663	3.4605	2.9273	2.7967	0.1306 (0.046)[24]	0
ATP-ACR	3.6170	3.2822	3.0404	2.6559	0.3845 (0.16)[25]	0.001
4CzIPN	3.2921	3.0897	2.7966	2.5038	0.2928 (0.083)[4]	0.1017
TPA-QNX(CN)2	3.4524	3.2238	2.9169	2.6097	0.3072 (0.111)[26]	0.1602
MFAc-PPM	3.6110	3.5283	3.0359	2.8503	0.1856 (0.25)[27]	0
DBQPXZ	3.4394	3.1283	2.9071	2.5343	0.3728 (0.0863)[28]	0
DFDBQPXZ	3.3436	3.1976	2.8353	2.5890	0.2463 (0.04)[29]	0
PXZPDO	3.1010	2.7940	2.6533	2.2701	0.3832 (0.04)[30]	0.0006

is mainly located in the range of 2.5-3.5 eV for all the seven types (Fig. 3). These candidates can be employed for OLED materials in various colours and there is no strong bias towards a certain energy range in this initial dataset. There is no relation between type and excitation energy. In the discussion below, we use the original CSD identifiers to refer to specific molecules.

In the first instance, it is expected to find some experimentally known TADF molecules which have the typical donor-acceptor (D-A) or D-A-D architectures. We found that 11 structures in the candidates were known as TADF emitters and three examples are shown in Fig. 4 and labelled them as Type I. We can see that both the conventional twisted D-A connection and the through-space charge transfer by homo-conjugation are identified by our HTVS process. Then, we observed that some D-A or D-A-D structures are formed by common TADF donors and acceptors but not reported as TADF materials (Type II, Fig.4). The electron-donor phenoxazine, 9,9-dimethyl-9,10-dihydroacridine, diphenylamine, carbazole, dihydrophenazine, N,N-dimethylbenzenamine, dimethylamine and the electron-acceptor phenylmethanone, pyrimidine, 1-nitrobenzene, 1,3,4-oxadiazole, pyrazine, sulfonyl units appear in these structures. One of the entries, SOHQAI is a host material for use in phosphorescent organic light-emitting diodes (PhOLEDs).[31] This indicates the bipolar host materials for PhOLEDs or TADF OLEDs could become the TADF emitters. TARNUW can be regarded as an example of the so-called "twin-emitter", which means two individual TADF molecules are connected through their donors or acceptors.[7] It has been revealed that the "twin-emitter" strategy can improve the thermal, optical and electron-optical properties of TADF emitters.[7] We label as Type III the chemical structures of D-A molecules which possess either a donor or an acceptor not considered in the TADF literature (Fig. 4). In ILUBEY, the bis(pentafluorophenyl)borane group serves as an acceptor and the 2,2,6,6-tetramethylpiperidine group plays a donor role. The borane-based group has previously been introduced in some TADF molecules.[32] It has been known that incorporation of halogen atoms can reduce the triplet lifetime and enhance the RISC process.[33] The Ph_3P=N group in HATXOP can be found in many selected "hits" and acts as an acceptor unit. The Ph_3P unit has been used in the development of Cu(I)-based TADF materials.[34] The related Ph_2P=O (diphenylphosphine oxide) group has been used as an electron-acceptor in nonlinear optical materials[35] and as bipolar dendrons in self-host TADF dendrimers.[36] In XOTCUF and WANTIQ, the 4,5-bis(ethylthio)-1,3-dithiole unit is identified as an excellent electron donor[37] but, to the best of our knowledge, it has not been used for TADF materials. This donor fragment is potentially very interesting for TADF systems (when connected with a corresponding acceptor) as it produced well separated HOMO and LUMO without introducing twisting (Fig. S5, ESI†). This indicates that the donor, acceptor and linker balance very well to obtain a small ΔE_{ST} in a coplanar molecular structure. We identified as Type IV structures that have a clear D-A character but are very remote from what is currently considered in the D-A chromophore literature (Fig. 4). More than one acceptor appears in these molecules. The donor and the acceptor are connected directly, by spiro junction, or even a combination of the two. These novel linkage modes open many new ways to arrange the donors and acceptors in TADF emitters. Although the "hits" of type I-IV satisfy the conventional D-A design strategies, most of them are not known as TADF materials and could provide insight for the design of new TADF emitters.

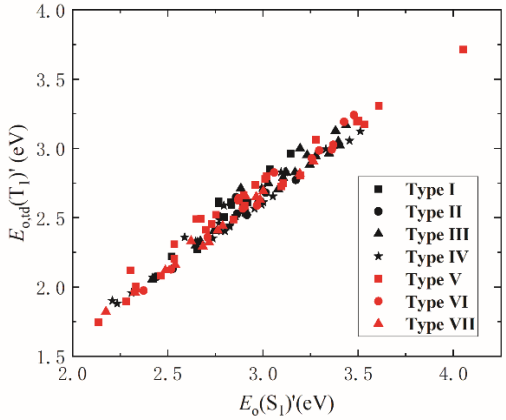

Fig. 3 The calibrated excitation energies of $E_o(S_1)'$ and $E_{o,td}(T_1)'$ for the selected 125 candidates.

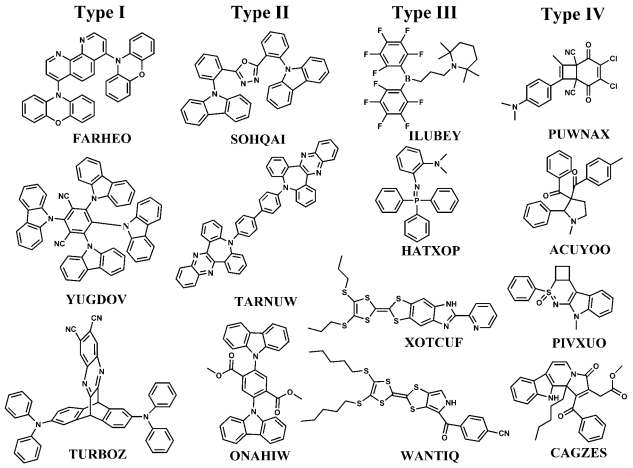

Fig. 4 Examples of D-A molecules satisfying the energy criterion for TADF resulting from the HTVS and classified as Type I: known TADF molecules, Type II: molecules formed by common TADF donors and acceptors, Type III: D-A molecule containing a novel donor or acceptor, and Type IV: molecules with a D-A character but non-standard chemical topology.

Now we focus on the molecules with structures that go beyond the established D-A design. We noticed that in the list of candidates there are many resonance zwitterionic structures which have strong charge-transfer characters. The anion part acts as a donor and the cation part can be regarded as an acceptor (Type V, Fig. 5). These anions and cations could provide candidate atoms for constructing novel TADF emitters by the multiple resonance effect, such as B and N atoms.[12] We also find that some candidates only include acceptors or donors and conjugated or non-conjugated linkers to form acceptor or donor molecules (Type VI, Fig. 5). The molecule denoted as JUNQUE would be normally considered as a donor because of its four N,N-dimethylbenzenamine groups but the two phenyl-phosphorous bonds in the central units impart an acceptor character onto this linker as shown in the molecular orbitals. In the other examples of this type, the chromophore is normally

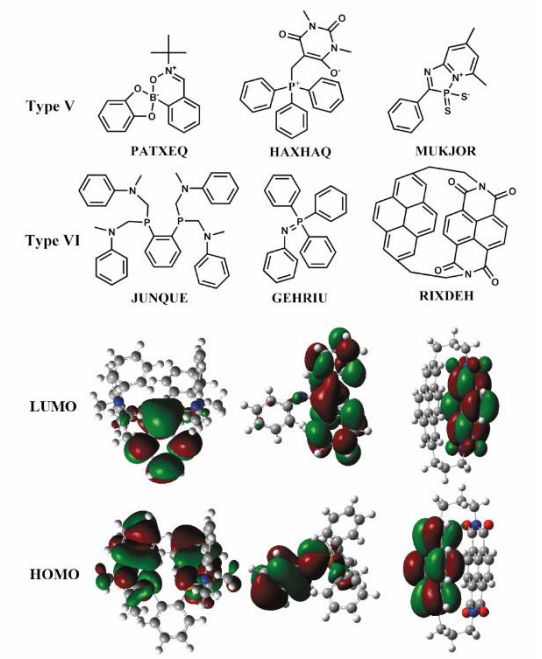

Fig. 5 Representative examples of molecules that are normally not characterized as D-A in literature and are labelled in the text as Type V: zwitterions and Type VI: donor or acceptor molecules. The frontier orbitals correspond to the Type VI molecules.

either a donor or an acceptor, but the linker can play the complementary role of acceptor or donor. Another interesting observation is that the Type VI molecule GEHRIU (Fig. 5) and Type III molecule HATXOP (Fig. 4) both contain the acceptor $Ph_3P{=}N$ group but the former has no corresponding donor. Moreover, their ΔE_{ST} and f are nearly equal each other. It seems to mean that the donor dimethylamine unit is not essential and the benzene ring which has weak donor character can keep balance with the acceptor $Ph_3P{=}N$ group. As there are Type III molecules including the acceptor $Ph_3P{=}N$ group, the role of the donor deserves to be revisited in more detailed studies. Another notable example is given by molecules like RIXDEH (Fig. 5), where a strong donor is forced by the molecular topology to be very close to a fragment without electron accepting functional groups but that act as an acceptor for the lowest excited state transition with charge transfer character.

The last group of molecules are the most surprising; as it is not easy to identify the donor or the acceptor moiety within them, they could not have been designed from the existing design rules and the explanation for their small ΔE_{ST} depend on the specific case. We label them as Type VII molecules, and we discuss four very different exemplars (Fig. 6). TUFWAS possesses a planar centre which is composed of two 1,3-dithiole units. The thiophene unit at the end is usually regarded as a π-bridge or a donor unit in organic semiconductors.[38] The electronic structure is quite peculiar with a LUMO orbital which possesses a σ symmetry and is dominated by the "bonding" interaction between the sulphur lone-pairs. The lowest energy transition is an unusual symmetry allowed HOMO→LUMO (π→σ) transition. The HOMO and LUMO are not in different regions of space but their overlap is small because the frontier orbitals have maxima/nodal planes in different regions. In the molecule

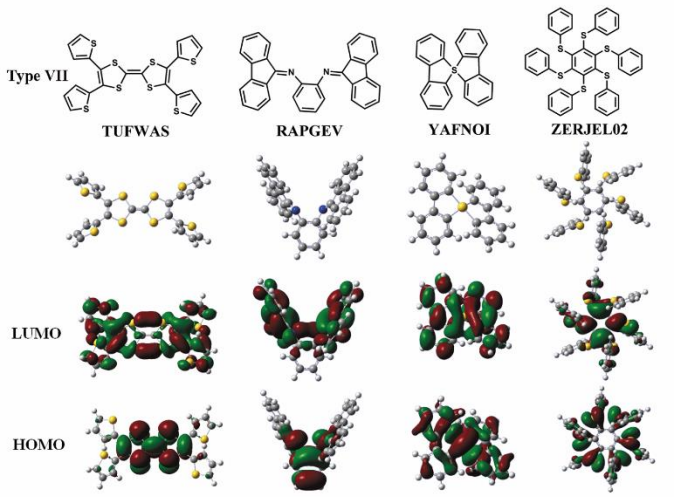

Fig. 6 Examples of Type VII molecules (without donor or acceptor) with their optimized geometries and frontier orbitals.

RAPJEV, the central phenyl linker acquires an unexpected donor character because of the substituent para (to be contrasted with the molecule JUNQUE (Fig. 5) where the substituents in para gave to the phenyl an acceptor character). Another uncommon feature is displayed by YAFNOI, a stable pentacoordinated sulphur compound with four S-C bonds.[39] It has an unusual bonding pattern with two apical S-C bonds, two equatorial S-C bonds, and the lone-pair electrons as the third equatorial position. Because of the residual lone-pair on sulphur the plane of the two conjugated fragments are tilted by a small angle of 29° unlike the 90° found in common spiro-compounds. The last example of this group is ZERJEL02, a persulfurated aromatic compound[40] consisting of a hexathio-benzene core and peripheral benzene substituents, which, as far as we know, has never been studied in TADF literatures. In this compound, the lowest energy exited state has a partial charge transfer character from the peripheral sulphur connection to the central benzene ring, with negligible change in overall dipole moment because of the high symmetry of the system. It has been found its analogues exhibit outstanding phosphorescence properties in solid state due to the well-known "Aggregation Induced Emission" (AIE) effects.[41] Nowadays AIE, which was discovered by Tang and coworkers,[42] has opened a way for development of versatile luminescent organic materials.[43-45] The AIE molecules are non-emissive when dissolved in dilute solvents but become highly luminescent when aggregated in the solid state. Specific structures, such as propeller-shaped tetraphenylethene and starburst triarylamine moieties, could avoid tight packing in the aggregated state and alleviate intermolecular π-π interaction, which commonly turns off light emission.[43] Hence, it is reasonable to predict that the asterisk-like ZERJEL02 could exhibit combined AIE and TADF properties and, in general, all our candidates with large steric hindrance may be considered for AIE-TADF applications.[7, 44]

The electron configuration of $S_0 \rightarrow S_1$ transition and the corresponding orbital overlap which means the overlap integral of norm of two orbitals[11] are analysed by using the Multiwfn software.[46] For comparison, the transition properties of some TADF molecules in Type I are also calculated (Table 2). The

$S_0 \rightarrow S_1$ transitions of these compounds are all mainly dominated by the HOMO→LUMO transition. Other electron configurations, such as HOMO→LUMO+2 for TUFWAS, also has a considerable contribution to the transition. For Type VII, the HOMO-LUMO orbital overlap, referred to as $O_{[H/L]}$, are much larger than those of TADF molecules. As a result, the ΔE_{ST} and f of Type VII are a little larger than those of Type I. RAPGEV and ZERJEL02 has a smaller HOMO-LUMO orbital overlap with respect to the other Type VII compounds, which is consistent with the orbital distribution plotted in Fig. 6.

Spin-orbital coupling, reorganization energy and adiabatic excitation energy

To establish whether the proposed candidates may have favourable excited state dynamics for TADF a more in-depth investigation was carried out. As we know, the intersystem crossing (ISC) and RISC rates are not only related to energy gap between S_1 and T_1 but also related to the SOC between singlet and triplet states.[47] The SOC constants were computed using the Dalton 2013 package.[48] We initially computed the SOC between S_1 and T_1 in the geometry of S_0 to see if this is a useful strategy to further rule out molecules that are clearly unsuitable because of a small coupling between states of different multiplicity. The full results are shown in the ESI (Table S1, ESI†), but in essence we find that for 84% (105/125) of the molecules the SOC is found below 10 cm^{-1}. Moreover, for the known TADF molecules (Type I) the SOC is very small (< 1 cm^{-1}). This variability is probably less important than the effect of reorganization energy and geometric relaxation in the excited state that are explored next.

The final step of the screening is to consider geometry optimization of S_1 and T_1 to estimate the energy barrier for ISC and RISC and to characterize the adiabatic excitation energy. This step is computationally extremely demanding and could be carried out on a representative sample of the candidates. A total of 28 candidates, which include the known TADF molecules and the ones with f>0.02 and SOC>0.1 cm^{-1} at S_0 geometry, are chosen to offer a good representation of various types. The S_1 and T_1 geometries were optimized by TDDFT method at M062x/def2svp level. The reorganization energies between S_1 and T_1 states $\lambda(S_1T_1)$ and between T_1 and S_0 states $\lambda(T_1S_0)$ were calculated. The reorganization energy here is defined as the average of the relaxation energies of related two states. The adiabatic excitation energy of S_1 state $E_{ad}(S_1)$, T_1 state $E_{ad}(T_1)$ and their energy difference ΔE_{ad_ST} were obtained. The SOCs were computed again based on the optimized S_1 and T_1 geometries respectively. The Marcus barrier for the RISC, which is equal to $E_M=[\lambda(S_1T_1)-\Delta E_{ad\_ST}]^2/[4\lambda(S_1T_1)]$,[49] is also calculated and reported in Table 3. Here, the Marcus barrier has the same meaning as the activation energy mentioned in some literatures.[13(a),50] This barrier is a key factor to control RISC. For the same ΔE_{ad_ST} values, large $\lambda(S_1T_1)$ could lead to large barrier for RISC process.[50(b)] Small Marcus barrier can speed up the RISC rate.

The reorganization energies $\lambda(S_1T_1)$ of the eight known TADF molecules (Type I) are not too large and the average value is around 0.263 eV (Table 3). For the 20 molecules of Type II-VII, the $\lambda(S_1T_1)$ are all less than 0.5eV. Moreover, among them 15 molecules have $\lambda(S_1T_1)$ lower than the average of TADF molecules, which indicates most of candidates have the $\lambda(S_1T_1)$ within the range of TADF molecules. But for the $\lambda(T_1S_0)$, the values of several candidates such as WAPLIJ and DEJMUC are much larger than those of the TADF molecules. Eight candidates in which the $\lambda(T_1S_0)$ is larger than 0.55eV could not be suitable for TADF candidates. The average value of ΔE_{ad_ST} for Type I molecules is about 0.257 eV, which is in a good agreement with the universally accepted upper limit for the efficient TADF emitters, 0.25 eV.[5(b)] For the predicted new TADF molecules, the calculated ΔE_{ad_ST} are also very small and within 0.25 eV except three molecules (Table 3). This demonstrates that our pre-screening procedure is a very efficient way to select candidates with small energy gap and the initial criterion of ΔE_{ST} <0.4 eV is suitable for selecting most of the potential TADF candidates. Encouragingly, all computed Marcus barriers E_M for the known TADF molecule are very low with the average 24 meV ($\sim k_BT$ at T=300 K), which can enhance the rate constant of electron transfer between T_1 and S_1 states in a simple Marcus theory picture.[49] It is found that nearly half of the novel proposed molecules share the similar kinetic parameter with the known TADF molecules.

In general, the $\langle S_1|H_{so}|T_1\rangle$ calculated on S_1 geometry is close to the value obtained by S_0 geometry (Table 3). The $\langle S_1|H_{so}|T_1\rangle$ of T_1 geometry is usually larger than that of S_1 geometry. The $\langle S_1|H_{so}|T_1\rangle$ of the known TADF molecules are very small and less than 1 cm^{-1} in three cases. The SOC values for some potential TADF candidates are a little larger than those of type I, but this is only due to our selection of molecules for in-depth study, from

Table 2 Calculated oscillator strength f, energy gap ΔE_{ST}, main electron configuration, and overlap between frontier molecular orbitals for two types candidates.

Type	CSD ID	f	ΔE_{ST}(eV)	Electron configuration	Orbital overlap
VII	TUFWAS	0.0098	0.3537	H→L: 57.4%; H→L+2: 36.9%	O[H/L]=0.59; O[H/L+2]=0.63
	RAPGEV	0.0005	0.3903	H→L: 76.6%; H-3→L+1: 9.4%	O[H/L]=0.38; O[H-3/L+1]=0.39
	YAFNOI	0.0804	0.3958	H→ L 79.3%; H→L+1: 16.4%	O[H/L]=0.59; O[H/L+1]=0.57
	ZERJEL02	0.0585	0.3547	H→L: 54.8%; H→ L+1: 36.0%	O[H/L]=0.45; O[H/L+1]=0.44
I	VENXAQ	0	0.2462	H→L: 64.0%; H→L+1:19.8%	O[H/L]=0.05; O[H/L+1]=0.10
	IVETAG	0	0.2196	H→L: 72.8%; H→L+1: 16.3%	O[H/L]=0.08; O[H/L+1]=0.10
	HIFJOY	0.0002	0.1823	H→L: 95.1%	O[H/L]=0.15
	FARHEO	0.0004	0.1479	H→L:79.3%; H→L+1: 16.4%	O[H/L]=0.19; O[H/L+1]=0.44

Table 3 Reorganization energies $\lambda(S_1T_1)$ and $\lambda(T_1S_0)$, adiabatic excitation energies $E_{ad}(S_1)$, $E_{ad}(T_1)$ and the energy difference ΔE_{ad_ST}, the Marcus barrier E_M, the SOC constants $<S_1|H_{so}|T_1>$ at the S_1, T_1 and S_0 geometries, and the SOC constants $<T_1|H_{so}|S_0>$ at the T_1 and S_0 geometries.

No.	CSD ID	$\lambda(S_1T_1)$ (eV)	$\lambda(T_1S_0)$ (eV)	$E_{ad}(S_1)$ (eV)	$E_{ad}(T_1)$ (eV)	ΔE_{ad_ST} (eV)	E_M (eV)	$<S_1\|H_{so}\|T_1>$ (cm^{-1})			$<T_1\|H_{so}\|S_0>$(cm^{-1})		Type
								S_1	T_1	S_0	T_1	S_0	
1	FARHEO	0.1654	0.3334	2.9284	2.8683	0.0601	0.0168	0.047	0.242	0.050	1.147	0.504	I
2	IVETAG	0.2435	0.3209	2.9902	2.8465	0.1437	0.0102	0.002	0.011	0.003	1.295	1.097	I
3	TURBOZ	0.1113	0.2543	3.2196	2.9700	0.2496	0.0430	0.011	0.029	0.011	0.395	0.330	I
4	BICQEM	0.3297	0.3804	2.7662	2.3808	0.3854	0.0024	0.008	0.404	0.013	1.142	1.231	I
5	HIFJOY	0.5004	0.4063	3.4563	3.2901	0.1662	0.0558	0.008	0.560	0.067	0.117	1.970	I
6	EXAMUN	0.3092	0.5337	3.3471	2.8785	0.4686	0.0205	0.007	0.368	0.002	1.235	1.644	I
7	TESJEJ	0.2603	0.4780	2.6992	2.2366	0.4626	0.0393	0.018	0.46	0.024	0.981	1.494	I
8	TEGVAF	0.1811	0.3276	2.9709	2.8539	0.1170	0.0057	0.029	0.145	0.049	1.656	1.774	I
9	IWOKUB	0.3246	0.6298	3.0483	2.3645	0.6838	0.0994	0.204	0.493	0.479	0.004	<0.001	II
10	VIHGAU	0.0038	0.4828	2.1743	2.1390	0.0353	0.0653	0.049	0.062	0.916	3.366	3.992	II
11	ILUBEY	0.0603	0.4432	3.1234	3.0695	0.0539	0.0002	0.255	0.797	0.197	1.116	0.305	III
12	IKUZET	0.1257	0.2690	2.4707	2.2214	0.2493	0.0304	0.161	0.300	0.224	0.838	0.630	III
13	HATXOP	0.0521	0.8883	2.7882	2.6004	0.1878	0.0884	2.563	6.592	1.395	7.445	3.543	III
14	XOTCUF	0.3928	0.3859	2.6983	2.6208	0.0775	0.0633	3.933	1.090	1.563	1.930	11.521	III
15	WANTIQ	0.0452	0.4752	2.4802	2.3626	0.1176	0.0290	1.759	2.426	1.548	7.254	6.312	III
16	PUWNAX	0.0554	0.5237	2.1585	1.9835	0.1750	0.0645	2.368	2.749	0.567	2.639	2.990	IV
17	FEJVAU	0.0882	0.3490	3.2010	3.0544	0.1466	0.0097	1.085	1.719	0.897	10.956	7.839	IV
18	AEPCNQ10	0.1072	0.5876	1.9658	1.8345	0.1313	0.0014	1.578	4.241	0.943	1.086	1.720	IV
19	CICGOK	0.4519	0.6710	2.2746	2.0365	0.2381	0.0253	2.013	8.982	5.363	7.832	12.664	IV
20	WAPLIJ	0.0196	1.3377	3.0944	2.9699	0.1245	0.1404	0.445	2.472	0.238	2.489	2.926	V
21	WOTCIR	0.0384	0.4492	2.8771	2.7434	0.1337	0.0591	0.446	0.649	0.711	0.500	1.479	V
22	VEBLIX	0.1663	0.4652	2.4770	2.1119	0.3651	0.0594	2.013	2.865	1.130	1.464	1.521	VI
23	RIXDEH	0.3103	0.4000	2.4300	2.0358	0.3942	0.0057	0.009	0.264	0.004	0.075	0.021	VI
24	GEHRIU	0.0060	0.9038	2.9538	2.8641	0.0897	0.2919	0.444	0.605	2.248	8.926	2.976	VI
25	DEJMUC	0.1433	0.9377	2.9217	2.7498	0.1719	0.0014	1.305	8.262	1.037	7.066	5.738	VI
26	LAHWUN	0.0157	0.7335	2.7039	2.6692	0.0347	0.0057	0.192	1.107	0.464	0.961	1.655	VI
27	MUHTOZ	0.0861	0.3185	2.6910	2.6080	0.0830	<0.0001	9.234	34.385	5.361	1.795	0.018	VII
28	RAPGEV	0.4369	0.3568	1.9548	2.0910	-0.1362	0.1879	5.183	4.989	0.621	1.173	14.476	VII

which we excluded cases with very small SOC. The SOC between T_1 and S_0 states $<T_1|H_{so}|S_0>$ which is related to the phosphorescence were also calculated based on T_1 optimized geometries. It shows that the $<T_1|H_{so}|S_0>$ values are all small and less than 15 cm^{-1}. These results are consistent with previous theoretical study on the SOC of TADF molecules.[47,13(a)] It seems that the variability SOC is not large, but small changes in SOC values can have important effects on the RISC rate.[13(a)] In the screening process, both SOC and ΔE_{ST} need to be considered.

It should be noted that many authors pointed out the important role of low-lying excited states other than T_1 and S_1[51] and that the role of non-radiative transitions has been ignored here. It is therefore likely that future screenings will have to include such effects or, alternatively, such effects are included in more detailed studies of fewer candidates emerging from these high-throughput screening. In addition, the packing mode in solid states will also affect the calculated values. In theoretical study, the molecular dynamics simulations and the combined quantum mechanics and molecular mechanics (QM/MM) method have been adopted to investigate the aggregation effects on optical properties for various luminescent organic materials including TADF and room-temperature phosphorescence (RTP) materials.[47(a), 52] Such effects could be explored in detailed for the potential candidates in the future. Finally, it would be preferable to identify computational methods that achieve similar of better accuracy without the need of experimental calibration.

Pathways toward molecular design

As shown in the previous sections, our virtual screening provides both confirmation of existing design rules and novel starting points for further investigations. The examples above are very different from each other; they represent only a small fraction of the novel structures and the underlying physical reasons for their potential TADF character is different. We expect that these findings can form the basis for an extensive experimental and theoretical investigation on these molecules to take place over the following years. In this work, we provide only a few illustrative examples of how some of the finding can be used to the design new molecules.

Based on several Type III and VII molecules, we performed a tentative design for TADF emitters with improving property. When the fluorine atoms of the bis(pentafluorophenyl)borane

group in ILUBEY are removed (Fig. 7), the calculated ΔE_{ST} increases significantly, from 0.1946 eV to 0.5872 eV. This demonstrates the fluorine atom has an important effect on TADF properties. If we use carbazole to replace the original donor, a new structure with a small ΔE_{ST} and a moderate f is obtained. Based on XOTCUF, two planar structures with slightly different acceptors are calculated. The structure satisfying the energy criterion with improved f can also be achieved. It is interesting to notice that WANTIQ has two isomers; one has a nearly linear backbone, and the other has a V-shaped conformation which corresponds to the X-ray structure (Fig. S6, ESI†). It is found that the linear structure has stronger oscillator strength due to the enhanced conjugation, but the ΔE_{ST} is larger than the energy criterion. Then we added more cyano units to modulate the charge transfer property. The results show that with the increase of cyano units, the ΔE_{ST} and the f decrease for both linear and V-shaped structures (Fig. S6, ESI†). The linear structure with three cyano units has a small ΔE_{ST} with a considerable f (Fig. 7). It has been known that the linear-shaped molecule is helpful for achieving high horizontal orientation, thereby enhancing the external quantum efficiency.[7] Therefore, it is expected that this structure could have better performance than the original WANTIQ molecule. Finally, we consider introducing different number of nitrogen atoms into the peripheral aromatic units of ZERJEL02, the energy gaps decrease significantly, but the oscillator strengths are still larger than 0.02 (Fig. 7). The HOMO orbitals of the designed molecules are more localized on the sulphur atoms (with respect to the original molecule) and a little farther away from the central benzene ring (Fig. S7, ESI†). This cause the orbital overlaps to decrease and the energy gap to be reduced.

Conclusions

Approximately seven hundred molecules with potential TADF activity have been identified from a database of 40000 excited state calculations of molecules contained in the CSD based on the energy gap and the oscillator strength. Then accurate quantum chemistry calculations have been performed and 125 potential TADF candidates have been extracted with the results of the screening benchmarked against measured excited state energies of TADF and non-TADF molecules. Finally, 28 candidates have been chosen for excited states dynamics calculations, and then the related parameters have been compared between the known TADF molecules and the predicted potential candidates. The goal of this work has been to perform a virtual search without imposing any predetermined design rules. Thanks to this choice, the identified potential candidates display a great diversity and could be used to initiate numerous lines of investigations. We classified our candidates in different types according to their "degree of novelty" with respect to the available TADF in literature. Besides the typical D-A structures, some novel donors, acceptors and molecular structures are identified. Furthermore, some molecule could not be constructed based on the existing D-A design rule and a fraction of them did not display a D-A character but different ways to realize a separation between HOMO and LUMO densities. Finally, we have briefly illustrated how the selected candidates open a "treasure box" for the design of new TADF materials.

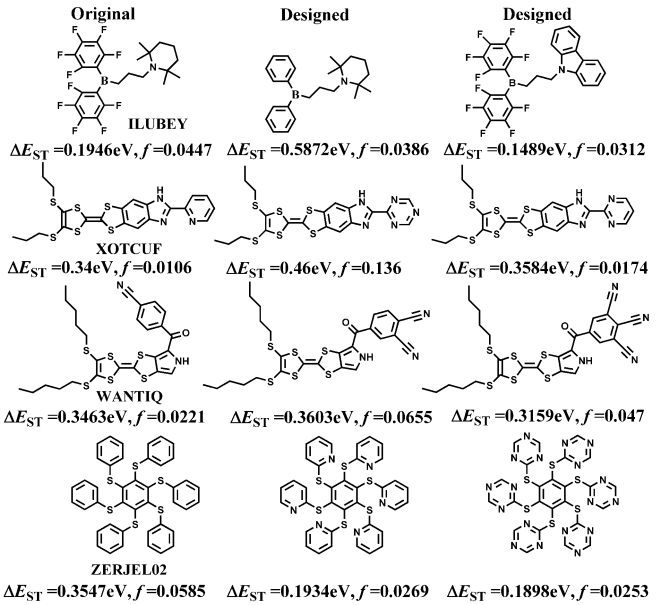

Fig. 7 Comparison of energy gap ΔE_{ST} and oscillator strength f between the designed structures and the original candidates.

Author Contributions

K. Z. performed all calculations, analysed the data, and wrote the paper. Ö. H. O. and T. N. prepared the calculation, compiled programs, and analysed the data. D. P. provided the calibration and assisted with analysing photophysical properties. A. T. designed and supervised the research and wrote the paper. All authors discussed the results and commented on the manuscript.

Conflicts of interest

There are no conflicts to declare.

Acknowledgements

We thank EPRSC and ERC for supporting this work. K. Z. thanks the support of the Natural Science Foundation of Shandong Province, China (Grant No. ZR2020MA078). D. P. gratefully acknowledges the Italian Ministry of Education, University, and Research (MIUR) for a Rita Levi Montalcini grant. We are grateful to T. Penfold (Newcastle) for useful suggestions.

Notes and references

1 A. Endo, K. Sato, K. Yoshimura, T. Kai, A. Kawada, H. Miyazaki and C. Adachi, *Appl. Phys. Lett.*, 2011, **98**, 083302.
2 Y. Tao, K. Yuan, T. Chen, P. Xu, H. Li, R. Chen, C. Zheng, L. Zhang and W. Huang, *Adv. Mater.*, 2014, **26**, 7931-7958.
3 Y. Im, M. Kim, Y. J. Cho, J.-A. Seo, K. S. Yook and J. Y. Lee, *Chem. Mater.*, 2017, **29**, 1946-1963.

4 H. Uoyama, K. Goushi, K. Shizu, H. Nomura and C. Adachi, *Nature*, 2012, **492**, 234-238.
5 (a) M. Y. Wong and E. Zysman-Colman, *Adv. Mater.*, 2017, **29**, 1605444; (b) D. S. M. Ravinson and M. E. Thompson, *Mater. Horiz.*, 2020, **7**, 1210-1217; (c) S. Huang, Q. Zhang, Y. Shiota, T. Nakagawa, K. Kuwabara, K. Yoshizawa and C. Adachi, *J. Chem. Theory Comput.*, 2013, **9**, 3872-3877.
6 Z. Yang, Z. Mao, Z. Xie, Y. Zhang, S. Liu, J. Zhao, J. Xu, Z. Chi and M. P. Aldred, *Chem. Soc. Rev.*, 2017, **46**, 915-1016.
7 X. Liang, Z.-L. Tu and Y.-X. Zheng, *Chem. Eur. J.*, 2019, **25**, 5623-5642.
8 (a) J. H. Kim, J. H. Yun and J. Y. Lee, *Adv. Optical Mater.*, 2018, **6**, 1800255; (b) T. Huang, W. Jiang and L. Duan, *J. Mater. Chem. C*, 2018, **6**, 5577-5596; (c) T. J. Penfold, F. B. Dias and A. P. Monkman, *Chem. Commun.*, 2018, **54**, 3926-3935; (d) L. Sun, W. Hua, Y. Liu, G. Tian, M. Chen, M. Chen, F. Yang, S. Wang, X. Zhang, Y. Luo and W. Hu, *Angew. Chem. Int. Ed.*, 2019, **58**, 11311-11316; (e) H. Wang, L. Xie, Q. Peng, L. Meng, Y. Wang, Y. Yi and P. Wang, *Adv. Mater.*, 2014, **26**, 5198-5204.
9 (a) Y. Zhang, H. Ma, S. Wang, Z. Li, K. Ye, J. Zhang, Y. Liu, Q. Peng and Y. Wang, *J. Phys. Chem. C*, 2016, **120**, 19759-19767; (b) H. Tanaka, K. Shizu, H. Nakanotani and C. Adachi, *Chem. Mater.*, 2013, **25**, 3766-3771; (c) K. Wu, T. Zhang, L. Zhan, C. Zhong, S. Gong, Z.-H. Lu and C. Yang, *Adv. Optical Mater.*, 2016, **4**, 1558-1566.
10 Y. Sagara, K. Shizu, H. Tanaka, H. Miyazaki, K. Goushi, H. Kaji and C. Adachi, *Chem. Lett.*, 2015, **44**, 360-362.
11 X.-K. Chen, Y. Tsuchiya, Y. Ishikawa, C. Zhong, C. Adachi and J.-L. Brédas, *Adv. Mater.*, 2017, **29**, 1702767.
12 T. Hatakeyama, K. Shiren, K. Nakajima, S. Nomura, S. Nakatsuka, K. Kinoshita, J. Ni, Y. Ono and T. Ikuta, *Adv. Mater.*, 2016, **28**, 2777-2781.
13 (a) P. K. Samanta, D. Kim, V. Coropceanu and J.-L. Brédas, *J. Am. Chem. Soc.*, 2017, **139**, 4042-4051; (b) J. Gibson and T. J. Penfold, *Phys. Chem. Chem. Phys.*, 2017, **19**, 8428-8434.
14 (a) B. K. Shoichet, *Nature*, 2004, **432**, 862-865; (b) S. Curtarolo, G. L. W. Hart, M. B. Nardelli, N. Mingo, S. Sanvito and O. Levy, *Nat. Mater.*, 2013, **12**, 191-201; (c) E. O. Pyzer-Knapp, C. Suh, R. Gómez-Bombarelli, J. Aguilera-Iparraguirre and A. Aspuru-Guzik, *Annu. Rev. Mater. Res.*, 2015, **45**, 195-216.
15 Y. Shu and B. G. Levine, *J. Chem. Phys.*, 2015, **142**, 104104.
16 R. Gómez-Bombarelli, J. Aguilera-Iparraguirre, T. D. Hirzel, D. Duvenaud, D. Maclaurin, M. A. Blood-Forsythe, H. S. Chae, M. Einzinger, D.-G. Ha, T. Wu, G. Markopoulos, S. Jeon, H. Kang, H. Miyazaki, M. Numata, S. Kim, W. Huang, S. I. Hong, M. Baldo, R. P. Adams and A. Aspuru-Guzik, *Nat. Mater.*, 2016, **15**, 1120-1127.
17 (a) E. O. Pyzer-Knapp, K. Li and A. Aspuru-Guzik, *Adv. Funct. Mater.*, 2015, **25**, 6495-6502; (b) S.-Y. Lu, S. Mukhopadhyay, R. Froese and P. M. Zimmerman, *J. Chem. Inf. Model.*, 2018, **58**, 2440-2449; (c) N. R. Goud, X. Zhang, J.-L. Brédas, V. Coropceanu and A. J. Matzger, *Chem.*, 2018, **4**, 150-161; (d) L. Wilbraham, R. S. Sprick, K. E. Jelfs and M. A. Zwijnenburg, *Chem. Sci.*, 2019, **10**, 4973-4984; (e) N. Martsinovich and A. Troisi, *J. Phys. Chem. C*, 2011, **115**, 11781-11792; (f) T. Nematiaram, D. Padula, A. Landi and A. Troisi, *Adv. Funct. Mater.*, 2020, **30**, 2001906.
18 C. R. Groom, I. J. Bruno, M. P. Lightfoot and S. C. Ward, *Acta Crystallogr. Sect. B: Struct. Sci.*, 2016, **72**, 171-179.
19 (a) D. Padula, Ö. H. Omar, T. Nematiaram and A. Troisi, *Energy Environ. Sci.*, 2019, **12**, 2412-2416; (b) Ö. H. Omar, D. Padula and A. Troisi, *Chem. Photo. Chem.*, 2020, **4**, 5223-5229; (c) T. Nematiaram and A. Troisi, *Mater. Horiz.*, 2020, DOI: 10.1039/D0MH01159B.
20 M. J. Frisch, et al., Gaussian, Inc., Wallingford CT, 2016.
21 R. Grotjahn, T. M. Maier, J. Michl and M. Kaupp, *J. Chem. Theory Comput.*, 2017, **13**, 4984-4996.
22 S. Wu, M. Aonuma, Q. Zhang, S. Huang, T. Nakagawa, K. Kuwabara and C. Adachi, *J. Mater. Chem. C*, 2014, **2**, 421-424.
23 Q. Zhang, D. Tsang, H. Kuwabara, Y. Hatae, B. Li, T. Takahashi, S. Y. Lee, T. Yasuda and C. Adachi, *Adv. Mater.*, 2015, **27**, 2096-2100.
24 W.-L. Tsai, M.-H. Huang, W.-K. Lee, Y.-J. Hsu, K.-C. Pan, Y.-H. Huang, H.-C. Ting, M. Sarma, Y.-Y. Ho, H.-C. Hu, C.-C. Chen, M.-T. Lee, K.-T. Wong and C.-C. Wu, *Chem. Commun.*, 2015, **51**, 13662-13665.
25 T. Takahashi, K. Shizu, T. Yasuda, K. Togashi and C. Adachi, *Sci. Technol. Adv. Mater.*, 2014, **15**, 034202.
26 K. Kawasumi, T. Wu, T. Zhu, H. S. Chae, T. V. Voorhis, M. A. Baldo and T. M. Swager, *J. Am. Chem. Soc.*, 2015, **137**, 11908-11911.
27 I. S. Park, H. Komiyama and T. Yasuda, *Chem. Sci.*, 2017, **8**, 953-960.
28 L. Yu, Z. Wu, C. Zhong, G. Xie, Z. Zhu, D. Ma and C. Yang, *Adv. Optical Mater.*, 2017, **5**, 1700588.
29 L. Yu, Z. Wu, G. Xie, C. Zhong, Z. Zhu, D. Ma and C. Yang, *Chem. Commun.*, 2018, **54**, 1379-1382.
30 K. Wu, T. Zhang, Z. Wang, L. Wang, L. Zhan, S. Gong, C. Zhong, Z.-H. Lu, S. Zhang and C. Yang, *J. Am. Chem. Soc.*, 2018, **140**, 8877-8886.
31 Y. Tao, Q. Wang, C. Yang, C. Zhong, K. Zhang, J. Qin and D. Ma, *Adv. Funct. Mater.*, 2010, **20**, 304-311.
32 (a) Y.-J. Lien, T.-C. Lin, C.-C. Yang, Y.-C. Chiang, C.-H. Chang, S.-H. Liu, Y.-T. Chen, G.-H. Lee, P.-T. Chou, C.-W. Lu and Y. Chi, *ACS Appl. Mater. Interfaces*, 2017, **9**, 27090-27101; (b) K. Suzuki, S. Kubo, K. Shizu, T. Fukushima, A. Wakamiya, Y. Murata, C. Adachi and H. Kaji, *Angew. Chem. Int. Ed.*, 2015, **54**, 15231-15235.
33 A. Kretzschmar, C. Patze, S. T. Schwaebel and U. H. Bunz, *J. Org. Chem.*, 2015, **80**, 9126-9131.
34 (a) G. Blasse and D. R. McMillin, *Chem. Phys. Lett.*, 1980, **70**, 1-3; (b) J. M. Busch, D. M. Zink, P. D. Martino-Fumo, F. R. Rehak, P. Boden, S. Steiger, O. Fuhr, M. Nieger, W. Klopper, M. Gerhards and S. Bräse, *Dalton Trans.*, 2019, **48**, 15687-15698.
35 K. Chane-Ching, M. Lequan, R. M. Lequan, C. Runser, M. Barzoukas and A. Fort, *J. Mater. Chem.*, 1995, **5**, 649-652.
36 X. Ban, W. Jiang, K. Sun, B. Lin and Y. Sun, *ACS Appl. Mater. Interfaces*, 2017, **9**, 7339-7346.
37 (a) K. Guo, K. Yan, X. Lu, Y. Qiu, Z. Liu, J. Sun, F. Yan, W. Guo and S. Yang, *Org. Lett.*, 2012, **14**, 2214-2217; (b) F. Meyers, J. L. Brédas and J. Zyss, *J. Am. Chem. Soc.*, 1992, **114**, 2914-2921.
38 (a) C. Lu and W.-C. Chen, *Chem. Asian J.*, 2013, **8**, 2813-2821; (b) J.-H. Tsai, C.-C. Chueh, W.-C. Chen, C.-Y. Yu, G.-W. Hwang, C. Ting, E.-C. Chen and H.-F. Meng, *J. Polym. Sci. Pol. Chem.*, 2010, **48**, 2351-2360; (c) P. Li, H. Zhang and A. Troisi, *J. Phys. Chem. C*, 2018, **122**, 23890-23898.
39 S. Ogawa, Y. Matsunaga, S. Sato, I. Iida and N. Furukawa, *J. Chem. Soc., Chem. Commun.*, 1992, 1141-1142.
40 M. Gingras, J.-M. Raimundo and Y. M. Chabre, *Angew. Chem. Int. Ed.*, 2006, **45**, 1686-1712.
41 (a) A. Fermi, G. Bergamini, R. Peresutti, E. Marchi, M. Roy, P. Ceroni and M. Gingras, *Dyes Pigm.*, 2014, **110**, 113-122; (b) G. Bergamini, A. Fermi, C. Botta, U. Giovanella, S. D. Motta, F. Negri, R. Peresutti, M. Gingras and P. Ceroni, *J. Mater. Chem. C*, 2013, **1**, 2717-2724.
42 J. Luo, Z. Xie, J. W. Y. Lam, L. Cheng, H. Chen, C. Qiu, H. S. Kwok, X. Zhan, Y. Liu, D. Zhu and B. Z. Tang, *Chem. Commun.*, 2001, **18**, 1740-1741.
43 Y. Hong, J. W. Y. Lam and B. Z. Tang, *Chem. Soc. Rev.*, 2011, **40**, 5361-5388.
44 F. Rizzo and F. Cucinotta, *Isr. J. Chem.*, 2018, **58**, 874-888.

45 (a) S. Kim, Q. Zheng, G. S. He, D. J. Bharali, H. E. Pudavar, A. Baev and P. N. Prasad, *Adv. Funct. Mater.*, 2006, **16**, 2317-2323; (b) J. Xue, Q. Liang, R. Wang, J. Hou, W. Li, Q. Peng, Z. Shuai and J. Qiao, *Adv. Mater.*, 2019, **31**, 1808242; (c) F. Ni, Z. Zhu, X. Tong, M. Xie, Q. Zhao, C. Zhong, Y. Zou and C. Yang, *Chem. Sci.*, 2018, **9**, 6150-6155; (d) M. Chen, W. Xie, D. Li, A. Zebibula, Y. Wang, J. Qian, A. Qin and B. Z. Tang, *Chem. Eur. J.*, 2018, **24**, 16603-16608; (e) F.-Q. Wang, K. Zhao, M.-Y. Zhu and C.-K. Wang, *J. Phys. Chem. B*, 2016, **120**, 9708-9715.

46 T. Lu and F. Chen, *J. Comput. Chem.*, 2012, **33**, 580-592.

47 (a) J. Fan, Y. Zhang, Y. Zhou, L. Lin and C.-K. Wang, *J. Phys. Chem. C*, 2018, **122**, 2358-2366; (b) G. Jiang, F. Li, J. Fan, Y. Song, C.-K. Wang and L. Lin, *J. Mater. Chem. C*, 2020, **8**, 98-108; (c) L. Lin, Z. Wang, J. Fan, C.-K. Wang, *Org. Electron.*, 2017, **41**, 17-25; (d) L. Lin, J. Fan, L. Cai and C.-K. Wang, *Mol. Phys.*, 2018, **116**, 19-28.

48 (a) K. Aidas, et al., "The Dalton quantum chemistry program system", *WIREs Comput. Mol. Sci.*, 2014, **4**, 269-284; (b) Dalton, *A molecular electronic structure program*, Release *Dalton2013.3*, (2013), see http://daltonprogram.org.

49 (a) R. A. Marcus, *Angew. Chem., Int. Ed.*, 1993, **32**, 1111-1222; (b) R. A. Marcus and N. Sutin, *Biochemisica et Biophysica Acta*, 1985, **811**, 265-322.

50 (a) Q. Peng, D. Fan, R. Duan, Y. Yi, Y. Niu, D. Wang and Z. Shuai, *J. Phys. Chem. C*, 2017, **121**, 13448-13456; (b) M. Saigo, K. Miyata, S. Tanaka, H. Nakanotani, C. Adachi and Ken Onda, *J. Phys. Chem. Lett.*, 2019, **10**, 2475-2480.

51 X.-K. Chen, D. Kim and J.-L. Brédas, *Acc. Chem. Res.*, 2018, **51**, 2215-2224.

52 (a) G. Sun, Y. Zhao and W. Liang, *J. Chem. Theory Comput.*, 2015, **11**, 2257-2267; (b) L. Zhan, Z. Chen, S. Gong, Y. Xiang, F. Ni, X. Zeng, G. Xie and C. Yang, *Angew. Chem. Int. Ed.*, 2019, **58**, 17651-17655.